Functional studies of the kidney of living animals using multicolor two-photon microscopy

KENNETH W. DUNN,[1] RUBEN M. SANDOVAL,[1] KATHERINE J. KELLY,[1]
PIERRE C. DAGHER,[1] GEORGE A. TANNER,[3] SIMON J. ATKINSON,[1]
ROBERT L. BACALLAO,[1,2] AND BRUCE A. MOLITORIS[1,2]
[1]*Department of Medicine, Division of Nephrology, Indiana Center for Biological Microscopy,*
[2]*Roudebush Veterans Administration Medical Center, and* [3]*Department of Cellular
and Integrative Physiology, Indiana University Medical Center, Indianapolis, Indiana 46202*

Dunn, Kenneth W., Ruben M. Sandoval, Katherine J. Kelly, Pierre C. Dagher, George A. Tanner, Simon J. Atkinson, Robert L. Bacallao, and Bruce A. Molitoris. Functional studies of the kidney of living animals using multicolor two-photon microscopy. *Am J Physiol Cell Physiol* 283: C905–C916, 2002. First published May 15, 2002; 10.1152/ajpcell.00159.2002.—Optical microscopy, when applied to living animals, provides a powerful means of studying cell biology in the most physiologically relevant setting. The ability of two-photon microscopy to collect optical sections deep into biological tissues has opened up the field of intravital microscopy to high-resolution studies of the brain, lens, skin, and tumors. Here we present examples of the way in which two-photon microscopy can be applied to intravital studies of kidney physiology. Because the kidney is easily externalized without compromising its function, microscopy can be used to evaluate various aspects of renal function in vivo. These include cell vitality and apoptosis, fluid transport, receptor-mediated endocytosis, blood flow, and leukocyte trafficking. Efficient two-photon excitation of multiple fluorophores permits comparison of multiple probes and simultaneous characterization of multiple parameters and yields spectral information that is crucial to the interpretation of images containing uncharacterized autofluorescence. The studies described here demonstrate the way in which two-photon microscopy can provide a level of resolution previously unattainable in intravital microscopy, enabling kinetic analyses and physiological studies of the organs of living animals with subcellular resolution.

fluorescence; multiphoton; in vivo

FLUORESCENCE MICROSCOPY has become an invaluable tool in biomedical research. The power of fluorescence microscopy has recently been extended by a unique combination of technical developments in fluorescent probe technology, photonics, and optics. Specific probes may be conjugated to newly developed fluorophores that span the spectrum of light, allowing the subcellular distribution of multiple molecules to be compared. New fluorescent probes, sensitive to a variety of physical parameters, permit quantitative physiological studies to be conducted within individual cells. New color variants of the green fluorescent protein (GFP) have been developed, providing researchers with the ability to compare the behaviors of multiple, endogenously expressed proteins within living cells and tissues.

The development of faster and more sensitive imaging systems has been instrumental to the rapid growth in studies of living cells. Studies of living cells not only permit evaluations of cell physiology and molecular dynamics; they also provide morphological data that are unaffected by questions of cell preservation. Studies of living cells have largely been limited to model systems: cultured cells, isolated primary cells, or freshly isolated tissue segments. It is always a concern that these experimental systems, while experimentally tractable, may not accurately represent the in vivo situation because they generally lack interactions with the supporting tissues, including the vasculature, nervous system, and extracellular matrix. In the end, the most meaningful behaviors of cells will be observed in living animals.

Unlike in vitro preparations, the thickness of intravital microscopy samples presents the microscope with a challenging optical situation in which out-of-focus blur and light scattering combine to compromise image resolution and contrast. The quality of microscopic images of thick tissues is improved by confocal microscopy, which rejects out-of-focus light. However, the aperture that provides optical sectioning also rejects scattered fluorescence from the in-focus plane so that confocal microscopy is capable of collecting images only tens of microns into biological tissues.

The recent development of two-photon microscopy (10, 11) has provided researchers with the means to collect high-resolution optical sections deep into biological tissues. Because two-photon fluorescence depends on the simultaneous absorption of two photons of light, fluorescence excitation occurs only at the focal point where the density of illuminating photons is highest. Because no out-of-focus fluorescence is generated, flu-

---

Address for reprint requests and other correspondence: Kenneth Dunn, Dept. of Medicine, Division of Nephrology, Indiana Univ. Medical Center, 1120 South Dr., FH 115, Indianapolis, IN 46202 (E-mail: kwdunn@iupui.edu).

orescence may be collected without a confocal aperture, thus increasing the ability to collect the fluorescence generated deep into light-scattering biological samples (5). The extended reach of two-photon microscopy has been applied to intravital studies of the morphology and physiology of the brain (6, 14, 19, 23, 37, 38), the metabolism of skin (25), the development and vascularization of tumors (2), and embryonic development (35).

Here we present examples of the way in which two-photon microscopy can be applied to intravital studies of kidney physiology and pathophysiology. Because of its intimate relationship to the vasculature, the kidney may be readily labeled by intravenous injection of fluorescent probes. Because the kidney is easily externalized without compromising its function, microscopy may be used to evaluate a variety of renal parameters. Previous intravital studies of the kidney have used conventional fluorescence, reflected light, and transillumination microscopy to study organic anion transport (36, 40), tubular obstruction (42), and the microcirculation and tubular fluid flow (12, 15, 41).

Two-photon microscopy offers significant advantages for physiological studies of the kidney. First, it provides high resolution, sufficient to characterize subcellular structures and events. Second, the extended optical sectioning of two-photon microscopy provides true three-dimensional information that is critical to interpreting the complex organization of the kidney (30). Our studies have identified a range of interesting and powerful new applications for intravital imaging of the kidney by multiphoton microscopy. These studies demonstrate that multiple fluorophores can be simultaneously excited by two-photon absorption, allowing comparison of multiple probes and simultaneous characterization of multiple parameters. This spectral information is also crucial to interpreting images containing uncharacterized autofluorescence.

MATERIALS AND METHODS

Animal models. All animal studies were conducted in conformity with the National Institutes of Health Guide for the Care and Use of Laboratory Animals. Male Munich-Wistar and Sprague-Dawley rats (200–250 g body wt), male control and Tie-2-GFP mice (26) at 8–10 wk of age, and heterozygous adult male Han:SPRD rats with autosomal dominant polycystic kidney disease (34, 40) were used as described below. Animals were anesthetized by using thiobutabarbital (Inactin) ~130 mg/kg body wt intraperitoneally (Sigma, St. Louis, MO). After assuring adequate anesthesia, a 10- to 15-mm lateral incision was made dorsally under sterile conditions. The kidney was exteriorized, and a 27-gauge (for rat) or 30-gauge (for mouse) cannula was then inserted into the tail vein for dye infusion. For studies in which ischemia was induced, the renal artery and vein were occluded with a nontraumatic microaneurysm clamp for 30 min. For studies in which the medullary region of the rat or mouse was imaged, a parenchymal window was cut through the avascular plane of the kidney. During all procedures, core body temperature was maintained by using a homeothermic table.

Fluorescent probes. Fluorescent probes were dissolved in isotonic saline and injected into rats in a 0.5 to 1.0-ml bolus over ~3 min. The total volume injected into mice was ~0.2 ml. The probes used in this study are summarized in Table 1, which also lists the amounts injected for each probe. Except as noted, imaging commenced within 5 min of injection. All probes were obtained from Molecular Probes (Eugene, OR).

Micropuncture procedure. Micropuncture studies were conducted as described before (39). Briefly, the anesthetized rat was placed on a heated animal board, and rectal temperature was monitored with a probe and kept at 37°C. Surgical procedures included a tracheotomy, cannulation of femoral artery and vein, and placement of the left kidney in a micropuncture cup. During surgery the rat was given 1 ml of a 6 g/100 ml bovine serum albumin solution in 0.9% NaCl, and this was followed by a constant intravenous infusion of isotonic saline at 3 ml/h. Micropuncture was accomplished at ×100 magnification by using a Leitz stereoscopic microscope. Proximal tubule lumens were punctured with sharpened 7 to 8-μm-tip diameter pipettes by using a Leitz micromanipulator. Solutions were slowly infused into tubules by applying pressure to the micropipette contents with a mercury level-

Table 1. *Fluorescent probes used in these studies*

Probe	Localization	Quantity (rat/mouse)
Hoechst 33342	Membrane-permeant DNA-binding probe. Intravenous injection labels nuclei of all cells of kidney.	500 μg/250 μg
Propidium iodide	Membrane-impermeant DNA-binding probe; labels nuclei of apoptotic and necrotic cells. Accessible to all cells of kidney after intravenous injection.	10 μg/not applicable
10,000 mol wt Dextran	Bulk fluid-phase marker that is freely filtered by the glomerulus following intravenous injection. Briefly found in vasculature, rapidly filtered into renal tubules. It is internalized into endosomes of proximal tubule where it accumulates in lysosomes.	3 mg/600 μg
500,000 mol wt Dextran	Bulk fluid-phase marker that is retained in the vasculature of animals with intact glomerulus following intravenous injection.	400 μg/100 μg
Bovine serum albumin	Bulk fluid-phase marker that is retained in the vasculature of animals with intact glomeruli following intravenous injection.	2 mg/not applicable
Texas red-gentamicin	Small molecular weight therapeutic antibiotic that is freely filtered across the glomerulus following intravenous injection. It is internalized into endosomes of proximal tubule cells where it then accumulates in lysosomes.	2 mg/not applicable
Rhodamine R6	Vital probe that accumulates in active mitochondria on the basis of membrane potential. Intravenous injection results in labeling of endothelia and circulating white cells.	2 μg/not applicable

ing bulb. The solutions were colored with 100 mg/dl lissamine green to observe fluid flow. Sudan black-stained castor oil was injected into nearby nephrons to aid in subsequent localization of the infused tubules. A careful drawing was made of the infused tubules in relation to tubules containing oil. The animal was transported to the stage of the two-photon microscope, the labeled nephrons were identified, and images were collected.

Microscopy. All imaging was conducted by using a Bio-Rad MRC-1024MP Laser Scanning Confocal/Multiphoton scanner (Hercules, CA) attached to a Nikon Diaphot inverted microscope (Fryer Co, Huntley, IL) with a Nikon ×60 1.2-NA water-immersion objective. Fluorescence excitation was provided by a titanium-sapphire laser (Spectraphysics, Mountain View, CA). After a range of excitation wavelengths was evaluated, the best results for stimulating fluorescence in triply labeled samples were obtained by using 800-nm excitation, which was used for all studies. Laser output was attenuated with neutral density filters to between 3 and 40% so that, after accounting for losses in the optical train of the microscope, we estimated that the power at the surface of the kidney was between 2 and 28 mW. Power at the focal point is harder to estimate because of absorption by the tissue but will be lower than these values, depending on the depth of imaging.

A water-circulating heating pad was placed on the stage ~1 h before image acquisition took place to heat the stage to 37°C. Animals were placed on the stage with the exposed kidney placed in a 50-mm-diameter coverslip-bottomed cell culture dish (Warner Instruments, Hamden, CT) bathed in isotonic saline (Fig. 1). The coverslip-bottomed dish was secured to the stage plate by applying adhesive tape to the bottom of the dish. To minimize motion, the animal was placed so the kidney was as close to the edge of the dish as possible, the chest being placed outside the dish to minimize movement of the kidney during image acquisition. The heating pad was then placed directly over the animal and supplemental oxygen was provided. Because of animal movement and respiration, images were collected rapidly in a single scan at either the "fast" or "normal" speed setting (providing acquisitions in ~0.5 and 1 s, respectively).

Image processing. In some cases, the noise inherent in the rapidly acquired images was reduced by applying a 3×3 low-pass filter to each image, with the use of Metamorph Image Processing Software (Universal Imaging, West Chester, PA). Final preparation of images, including adjustments in brightness and contrast, was conducted with Adobe Photoshop (Adobe, Mountain View, CA).

Rotated volume renderings were produced by using Voxx volume rendering software developed by the Indiana Center for Biological Microscopy (7). The real-time renderings produced with Voxx were then recorded as movies by using Adobe Premiere (Adobe, Mountain View, CA), which was also used to produce the time series movies. Palette mapping functions in Voxx software were also used to enhance the contrast of rendered volumes.

Although the colors shown in the figures are similar to the "true" colors of probe fluorescence, they are digital reconstructions. As discussed above, 800-nm illumination stimulates a broad spectrum of fluorescence in triply labeled samples. This spectrum of fluorescence is split into three channels, centered at 605, 525, and 455 nm, which are then collected in separate photomultiplier tube detectors. These three channels, displayed as pure red, green, and blue, respectively, are then recombined in the color images. In some cases, the contrast and brightness of each color was further adjusted for clarity.

Because of the photomultiplier tubes were adjusted differently for each experiment, the hue of specific objects in the images varies slightly between experiments. For example, the brown autofluorescent inclusions of proximal tubule cells (discussed below) may appear more reddish or yellowish, depending on how the photomultiplier settings for the "red" and "green" channels are adjusted.

RESULTS

DNA stains can be used as intravital labels of cell nuclei in the kidney and to identify necrotic or apoptotic cells. Examples of intravital imaging of the kidneys of rats injected with Hoechst 33342 and propidium iodide are shown in Fig. 2. Hoechst 33342, a cell-permeant DNA-binding dye, is rapidly distributed throughout the kidney after tail-vein injection and brightly labels nuclei of the endothelia, circulating leukocytes, the glomerulus, interstitial cells, and the different renal epithelial cells. Propidium iodide is a membrane-impermeant DNA-binding probe that is excluded from living cells and can thus be used to identify dead or dying cells with a compromised plasma membrane. By
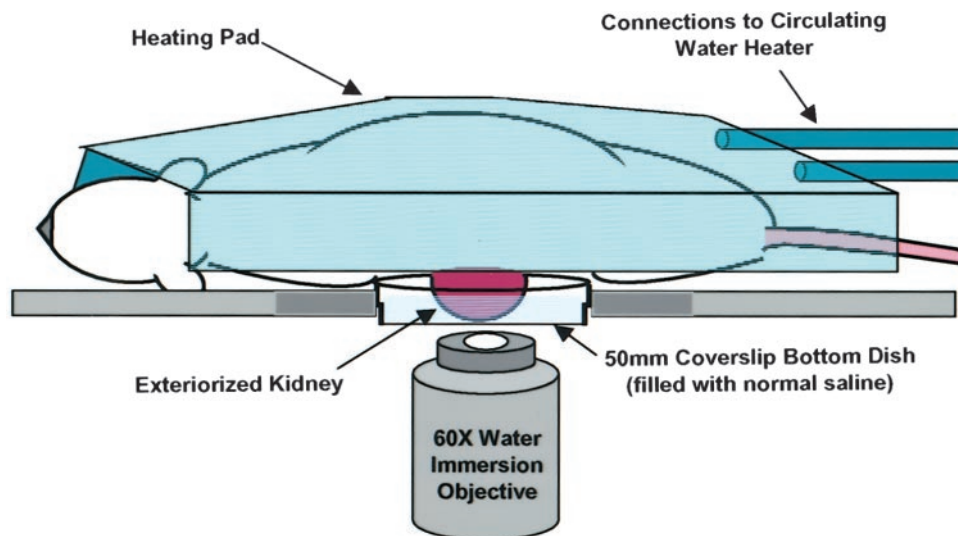

Fig. 1. Diagram of experimental setup used for intravital imaging of live rodent kidneys. Animals were anesthetized and prepared as described in MATERIALS AND METHODS and then placed on the stage of an inverted microscope with the exposed kidney placed in a 50-mm coverslip-bottomed cell culture dish bathed in normal saline. The heating pad was then placed directly over the animal. Imaging was conducted with the use of a Nikon ×60 1.2-NA water-immersion objective.

Fig. 2. DNA stains can be used as intravital labels of cell nuclei in the kidney and to identify necrotic or apoptotic cells. *A* and *B*: projections of image volumes (each ~50 μm thick) from the superficial cortex of rat kidneys. The volume shown in *A* was collected from a normal rat injected with propidium iodide and Hoechst 33342. The volume shown in *B* is similar, except that it was collected from a rat subjected to 30 min of unilateral renal ischemia produced by renal pedicle clamping. After 24 h of recovery, propidium iodide and Hoechst 33342 were injected intravenously. Necrotic and apoptotic nuclei in the ischemic kidney appear white (arrows), due to the combination of Hoechst and propidium iodide fluorescence. Note that these volumes are better appreciated as Voxx-rendered animations that may be viewed as Movies 2*a* and 2*b* (Supplementary Material for this article may be viewed online). *C* and *D*: single focal plane images collected from the kidney of a rat subjected to brief (30 min) ischemia with 24-h recovery. Whereas the image of the cortex (*C*) shows little evidence of cell death, numerous dead cells are apparent in the image of the outer medulla (*D*). As described in text, large arrows indicate nuclei of necrotic cells, small arrows indicate the condensed nuclei of cells at early stages of apoptosis, and arrowheads indicate the nuclei of cells at later stages of apoptosis, whose labeling with propidium iodide reflects secondary necrosis. The medullary region was examined in an animal after preparation of a parenchymal window. Scale bar = 40 μm.
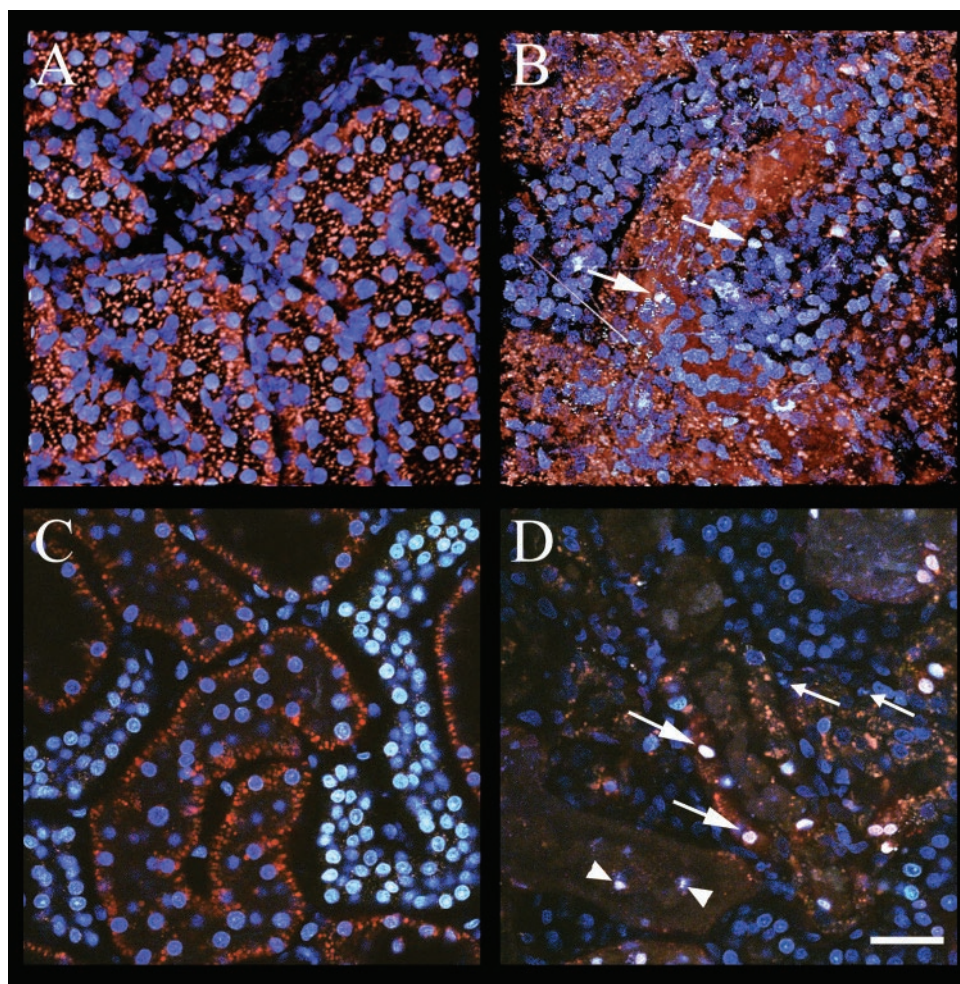
injecting an animal with both probes, one can determine the fraction of necrotic cells in a tissue from the proportion of nuclei labeled with Hoechst that are also labeled with propidium iodide (identified by the white fluorescence that results from the combined contributions of blue Hoechst and orange propidium iodide fluorescence).

Figure 2*A* shows a projection of a 50-μm-thick volume collected from the superficial cortex of the kidney of a control animal, whereas Fig. 2*B* shows the projection of a similar volume collected from an animal after 30 min of renal ischemia and 24 h of reperfusion. These volumes are better evaluated as animations of volume renderings. Please refer to the Supplementary Material[1] for this article (published online at the *American Journal of Physiology-Cell Physiology* web site) to view renderings (Movies 2, 3, and 5). Whereas the control kidney showed no evidence of dead cells, the postischemic kidney contained numerous dead cells with nuclei labeled with both dyes. In both cases, proximal tubules were found to contain punctate structures with an endogenous brown autofluorescence. In the postischemic kid-

ney, brown autofluorescence was also observed in what appear to be protein casts in the tubule lumens.

The working distance of the Nikon ×60 water-immersion objective limits imaging depth to 200 μm into kidney tissues. With Munich-Wistar rats, this distance is sufficient to image proximal tubules, distal tubules, and superficial glomeruli in intact kidneys placed on the microscope coverglass. Preparation of a posterior parenchymal window allowed imaging of the medulla. A comparison of cell death in the cortex and the medulla following ischemia is shown in Fig. 2, *C* and *D*, respectively. These images show that, consistent with previous studies (18), ischemia more severely affects the medulla, which was littered with numerous dead cells in both the walls of the tubules and in the cellular debris of the tubule lumens.

The ability to collect three colors of fluorescence was key to the interpretation of these studies, allowing distinction of four types of cells (Fig. 2*D*). Viable cells were identified by their intact nuclei that lack propidium iodide labeling. The nuclei of necrotic cells were similar in morphology but were accessible to propidium iodide (large arrows). Cells in the early stages of apoptosis, whose plasma membrane was still intact, can be identified by their characteristically fragmented and

---

condensed nuclei that were nonetheless inaccessible to propidium iodide (small arrows). As the plasma membrane integrity of apoptotic cells was lost as they progressed into secondary necrosis, these fragmented nuclei became increasingly labeled with propidium iodide (arrowheads).

Finally, the punctate autofluorescent structures of the proximal tubule cells were easily distinguished by their characteristic fluorescent signature. Color imaging was thus crucial to identifying DNA fluorescence, particularly after ischemia, when fragmented nuclei were frequently similar in size and shape to the autofluorescent structures but distinct in color.

Bulk fluid-phase probes can be used to evaluate renal fluid dynamics intravitally. Intravital fluorescence microscopy has been used to assess blood flow in the liver (8, 43), brain (17), bone (46), and developing tumors (44). Similar studies of the kidney have largely used a split hydronephrotic rat kidney model, in which tubular atrophy results in a thin tissue preparation suitable for wide-field transillumination microscopy (4, 12). In the interest of developing an experimental system that better models urinary flow, Heuser et al. (15) used epifluorescence microscopy to evaluate cortical blood flow in normal kidneys. Recently, Brown et al. (2) demonstrated the value of multiphoton microscopy in a study of blood flow deep into intradermal tumors.

We have used multicolor two-photon microscopy of animals injected with fluid-phase probes to characterize bulk fluid flow through the kidney of living animals. As outlined below, these studies demonstrate how bulk tracers may be used to assess capillary blood flow, glomerular filtration, fluid transport, and tubular solute concentration. In addition, the bulk tracer dextran can be used to characterize endocytosis by proximal tubule cells (22).

Figure 3*A* shows a microscope field collected from the kidney of a rat that had been injected with a combination of Hoechst 33342, rhodamine-conjugated albumin, and 10,000 mol wt fluorescein-conjugated dextran. The blue Hoechst fluorescence labeled the nuclei of all cells in the field. The red fluorescence of the albumin conjugate was limited to the capillaries in this field, whereas the small dextran was freely filtered into the tubule lumens. The filtered green dextran was then internalized into punctate endosomes by proximal tubule cells. This image is a single frame from a series of images collected over ~20 s. This time series is shown as Movie 3*a*. Circulating blood cells, which exclude the rhodamine albumin, appear as moving shadows in this animation. Significant heterogeneity in blood flow can be seen in this field, as reflected by the elongated shadows of blood cells in regions of high flow and the nearly normal profiles of blood cells in regions of lower flow.

A similar preparation is shown in Fig. 3*B*, which shows a field collected from an animal that had been injected with a combination of Hoechst 33342 and a 500,000 mol wt fluorescein-conjugated dextran. The large dextran was not filtered by the glomerulus but remained in the vasculature, labeling the peritubular and glomerular capillaries. The 30-s time series from which this image was selected is shown as Movie 3*b*. As above, blood flow through this field was highly variable, with regions of high and low flow characterized by blood cell profiles that are long or short, respectively. The punctate brown autofluorescence of proximal tubule cells is especially obvious in this field.

These preparations can also be evaluated over time to track the progress of a small molecule from the blood, across the glomerulus, to proximal tubules, and then to the distal tubules. Figure 3*C* shows an example of an optical section of a rat kidney 14 min after injection of Hoechst 33342, 500,000 mol wt fluorescein-conjugated dextran, and 10,000 mol wt rhodamine dextran. The large green dextran was limited to peritubular capillaries, but the small dextran was filtered by the glomeruli into the renal tubules. At this time point, the small red dextran was found at moderate levels in the lumen of the proximal tubule, identified by their endocytic uptake of the red probe, and at very high concentrations in the lumen of distal tubules. A similar field, shown in Fig. 3*D*, shows that after another 11 min, the red dextran had largely cleared from the lumen of the proximal tubule and was then concentrated in the lumen of distal tubules. The characteristic avid endocytosis of the proximal tubule epithelium is reflected in the bright punctate accumulation of the filtered red dextran in endosomes in cells of the proximal tubule. Such uptake was not observed in cells of the distal tubule. Unlike most other specimens, this particular rat showed a striking lack of punctate autofluorescence. Although we are interested in cultivating this characteristic in experimental animals, we have been unable to reproducibly reduce proximal tubule autofluorescence.

Similar results were obtained in studies of mice. Figure 3*E* shows an optical section from a mouse that had been injected with 500,000 mol wt fluorescein-conjugated dextran and 10,000 mol wt rhodamine dextran. As in rats, the large dextran was retained in the vasculature, whereas the small dextran was rapidly filtered into the renal tubules, accumulated in endosomes of the proximal tubule, and was concentrated in the lumen of distal tubules.

Phillips et al. (30) used three-dimensional two-photon imaging to evaluate the distended morphology of renal tubules in fixed tissue from a mouse model of polycystic kidney disease. We used intravital imaging to characterize the tubular morphology of the heterozygous Han:SPRD rat model of polycystic kidney disease (34, 40). Figure 3*F* shows a projection of a 90-μm-deep volume of the kidney of an animal that had been injected with Hoechst 33342 and 10,000 mol wt rhodamine dextran. This volume is better appreciated in the animated rendering shown as Movie 3*f*. The filtered red dextran clearly delineated the characteristic distended morphology of the tubules of this animal, a morphology very similar to that observed in the mouse model characterized by Phillips et al. (30). The rapid appearance of the dextran in this cystic structure also demonstrates that this cyst was connected to a func-

tioning glomerulus. The aberrant morphology shown in Fig. 3*F* is especially obvious when compared with Fig. 3*D*, which is presented at the same magnification.

Filtration and receptor-mediated endocytosis of the aminoglycoside gentamicin can be followed over time. As demonstrated above, we observed significant nonspecific uptake of fluorescent dextrans by the proximal tubule epithelium. We also evaluated the process of receptor-mediated endocytosis by proximal tubule cells, taking advantage of the megalin-mediated endo-

cytic uptake of aminoglycoside antibiotics. Figure 4*A* shows a high magnification image of the kidney of a rat that had been injected 11 min earlier with a Texas red conjugate of the aminoglycoside gentamicin. This fluorescent conjugate has been extensively characterized by our laboratory and was instrumental in delineating a novel pathway of aminoglycoside trafficking from the surface membrane directly to the Golgi complex (32, 33). The fluorescent gentamicin can be seen in the lumen of a proximal tubule in the center of the image
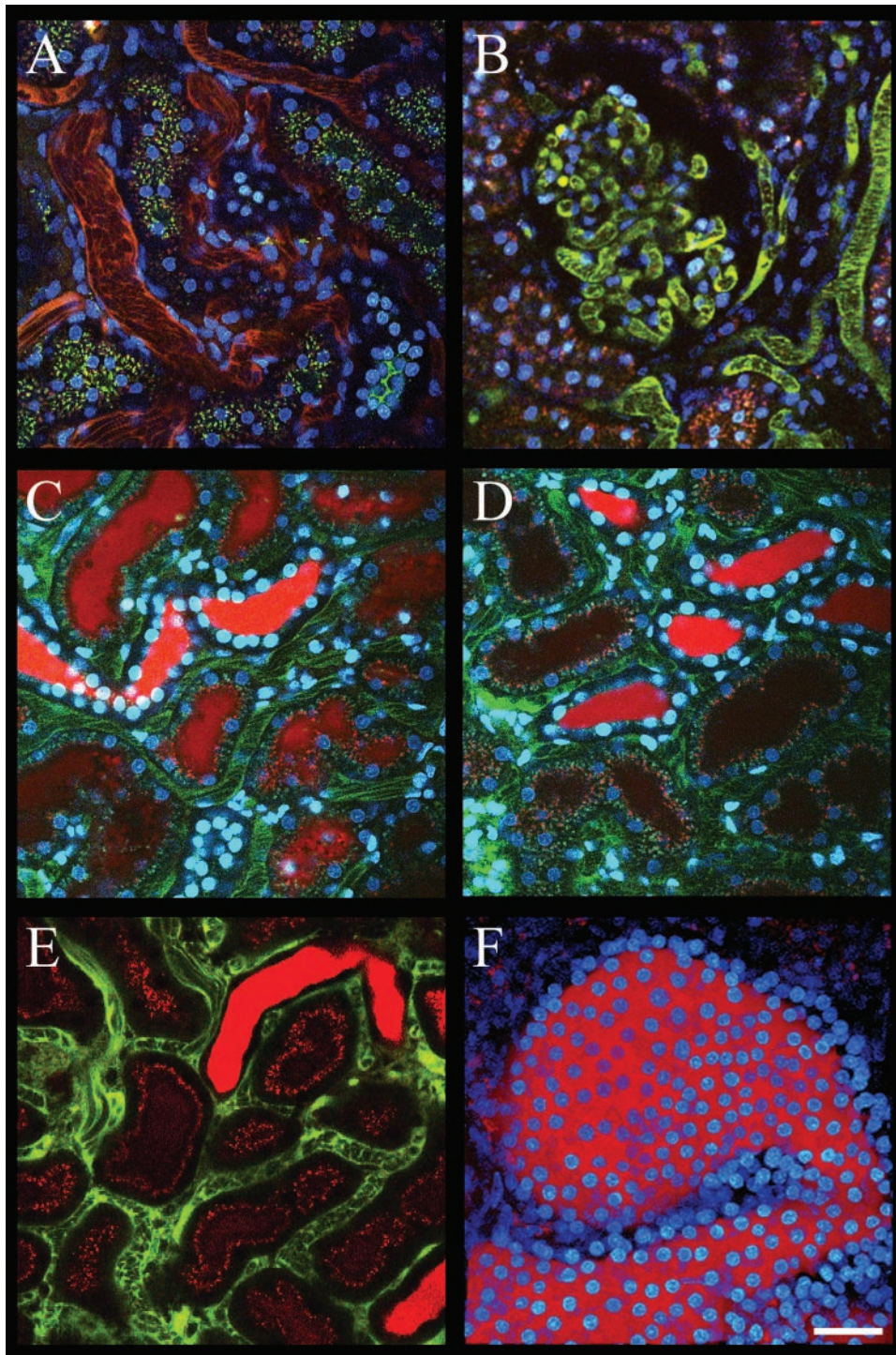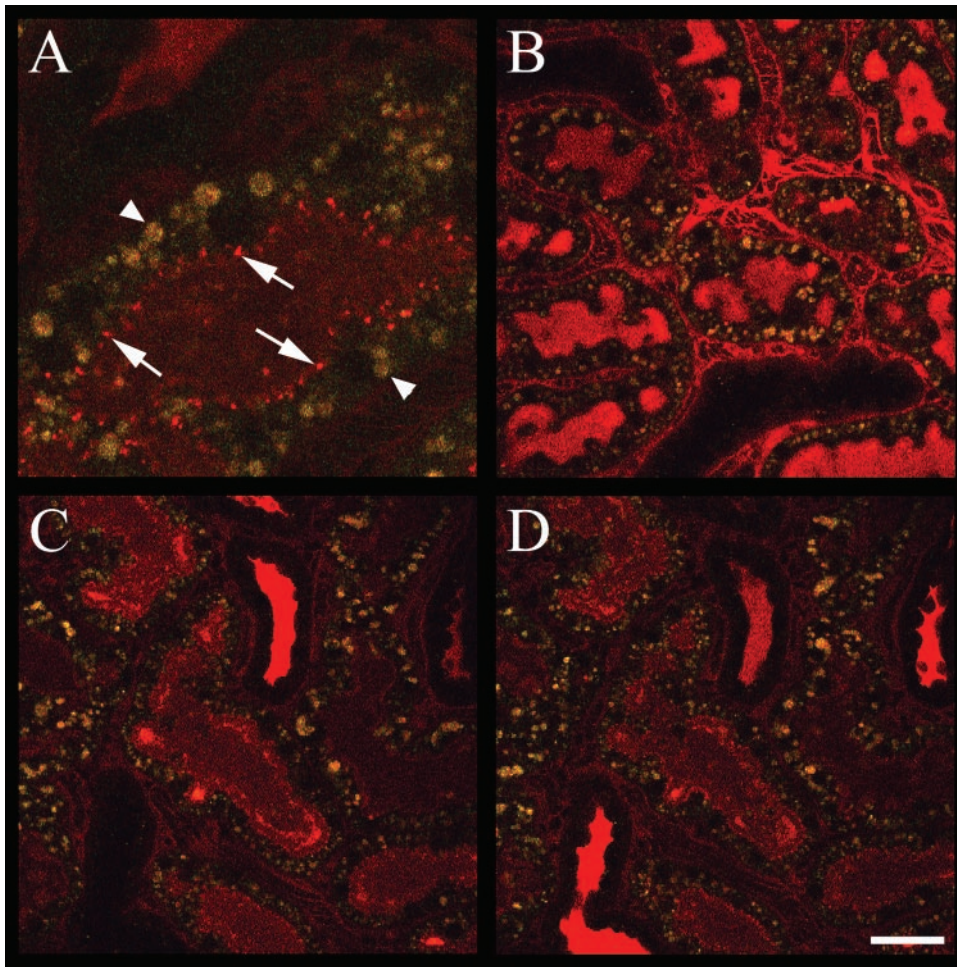
Fig. 4. Time series of Texas red-gentamicin transport in the intact rat kidney. *A*: high magnification image of a kidney of a rat collected intravitally 11 min after intravenous injection of Texas red-conjugated gentamicin into the tail vein. Gentamicin can be seen dimly labeling the lumen of the proximal tubule at the center of the field and brightly labeling endosomes where it has accumulated (arrows). Arrowheads indicate punctate brown autofluorescent structures at the base of proximal tubule cells. *B*: microscope field collected within 1 min of injection of Texas red-gentamicin, showing strong labeling of peritubular capillaries running between the tubular segments, as well as the lumen of proximal tubules (identified by their distinctive punctate brown autofluorescence). *C*: field collected within 3 min of injection, showing that gentamicin has been largely cleared from the blood and from the proximal tubule, and has reached the lumen of two distal tubule segments at the top of the field. *D*: the same field collected in *C* 1 min later, during which time the bolus of gentamicin has begun to clear the distal tubule segments previously labeled and has now reached new segments at the bottom and right side of the field. Scale bar = 40 μm except for *A*, where scale bar = 13 μm.

and accumulated in brightly labeled punctate endosomes at the apices of the proximal tubule epithelium. In this case, the proximal tubule can be identified not only by its endocytic uptake but also by the brown autofluorescent inclusions located basally in each cell. Close examination of this image also shows fluorescent gentamicin in the lumen of a distal tubule segment (Fig. 4*A*, *top left*) and in two capillaries running diagonally from bottom left to top right.

Transit of intravenously injected Texas red-gentamicin from the blood to the proximal tubule and to the distal tubule occurs very rapidly following tail vein injection. One min after injection, gentamicin was largely found in blood vessels but had already accessed the lumens of proximal tubules (Fig. 4*B*). Within 3 min, gentamicin had begun to clear from proximal tubule segments and to accumulate in the lumens of distal tubules, which can be identified by the lack of punctate

Fig. 3. Bulk fluid-phase probes can be used to evaluate renal fluid dynamics intravitally. *A*: image collected from a living rat that had been injected with Hoechst 33342, rhodamine-conjugated albumin, and 10,000 mol wt fluorescein-conjugated dextran. The 20-s time series from which this image was obtained is shown as Movie 3*a*. In the cross section shown in this field, intertubular capillaries (containing red-fluorescing albumin) are seen running between proximal tubule segments (containing punctate green fluorescence of fluorescein-dextran internalized into endosomes) and distal tubules (which lack endosomal dextran but show lumenal accumulation, *bottom right*). *B*: image collected at the level of the glomerulus from a living Munich-Wistar rat that had been injected with Hoechst 33342 and a 500,000 mol wt fluorescein conjugated dextran. The 30-s time series, from which this image was selected, is shown as Movie 3*b*. In this time series, blood flow through the glomerulus is apparent from the shadows of circulating cells moving in the green-fluorescing volume of the blood. *C*: image collected from the kidney of a living rat 14 min after injection of Hoechst 33342, 500,000 mol wt fluorescein-conjugated dextran, and 10,000 mol wt rhodamine dextran. A similar field, collected after another 11 min, is shown in *D*. In this and the following field (*E*), the green fluorescence of fluorescein dextran labels the peritubular capillaries running between proximal tubule segments (containing punctate red fluorescence of endosomal rhodamine dextran) and distal tubules (which lack endosomal uptake but show a lumenal accumulation of rhodamine dextran). *E*: mouse kidney image following injection with 500,000 mol wt fluorescein-conjugated dextran and 10,000 mol wt rhodamine dextran. *F*: projection of a 90-μm-deep image volume collected from the kidney of a living heterozygous Han:SPRD rat with polycystic kidney disease following intravenous injection with Hoechst 33342 and 10,000 mol wt rhodamine dextran. This volume is also presented as Movie 3*f*. Scale bar = 40 μm.

cellular autofluorescence (Fig. 4*C*). Comparison of this image with an image of the same field collected 1 min later (Fig. 4*D*) showed that during this minute, the bolus of gentamicin had reached a distal tubule segment previously lacking probe (*bottom left*) and had started to strongly accumulate in another segment at the *top right* of the field.

Although only a single fluorescent probe was used in these studies, the ability to collect multicolor images was again critical to their interpretation. The characteristic color signature of the punctate autofluorescence facilitated identifying proximal tubule cells and also clearly distinguished the autofluorescent bodies from Texas red-gentamicin-labeled endosomes.

Fluorescent indicators can be used to evaluate vitality of individual cells within animals. In Fig. 4*A* we showed an example of the use of two-photon microscopy to collect high-resolution images of individual endosomes within the cells of a living animal. As with cultured cells, cell-permeant probes can be used to label intracellular compartments in living animals. Rhodamine 6G, a fluorescent probe that accumulates in mitochondria due to membrane potential, has been used to track leukocytes in numerous intravital studies, including studies of kidney (15). Figure 5*A* shows a field collected from a living rat injected with a closely related mitochondrial probe, rhodamine R6. Similar to the results of Heuser et al. (15), we found that rhodamine R6 labeled the circulating white cells but labeled endothelial cells as well, where it accumulated in perinuclear mitochondria (red fluorescence adjacent to elongate endothelial nuclei). As expected, mitochondrial accumulation of rhodamine R6 dissipated in an animal whose kidney had been clamped to induce ischemia (data not shown). Intravenously administered rhodamine R6 also brightly labeled mitochondria of the glomerular capillaries (data not shown) but did not label the mitochondria of renal tubule cells.

Circumventing the problems of intravenous delivery of fluorescent probes/micropuncture delivery to renal tubules and the use of GFP. While for some studies we are interested in how intravenously administered probes are transported through the kidney, frequently it is necessary to characterize a particular type of cell. As described above, we have found that intravenous administration of some probes (e.g., Hoechst 33342) is sufficient to label an array of cell types in the kidney, but intravenous injection of other probes (e.g., rhodamine R6) results in labeling of only a subset of kidney cells. Therefore, the delivery of fluorescent probes to the cells of interest is a concern for many studies of living animals.

In the case of kidney tubules, probes that would not pass the glomerular filtration barrier can be delivered to kidney tubules via micropuncture delivery (39, 41). Figure 5*B* shows a field collected from the kidney of a rat approximately an hour after micropuncture injection of 500,000 mol wt fluorescein dextran into the lumen of a proximal tubule. In the proximal tubular segment shown in Fig. 5*B*, the injected dextran has been internalized into endosomes of proximal tubule cells. Because the micropuncture procedure was con-

ducted on a separate microscope stand, finding the labeled segment was facilitated by marking the region of the microinjected tubules with Sudan black-stained castor oil that was visible to the naked eye. The fluorescence of the stained oil can be seen in the lumens of several adjacent tubule segments.

One way of specifically labeling a particular population of cells is to utilize transgenic animals expressing GFP in a cell-specific manner. Figure 5*C* shows a projection of a three-dimensional image volume collected intravitally from a mouse expressing GFP driven by the Tie-2 promotor, which is restricted to endothelial cells (26). The green fluorescence of GFP can be seen in the cytosol of the endothelia of this 50-μm-thick volume, which is better appreciated as an animated rendering (Movie 5*c*). This volume also shows the same punctate brown autofluorescence seen in previous images of rat proximal tubule cells.

Expression of GFP by the leukocytes of an animal can be accomplished by transplantation with bone marrow cells expressing GFP. Figure 5*D* shows a microscope field collected intravitally from the kidney of a mouse that had been transplanted with bone marrow cells transduced with a retroviral vector expressing enhanced GFP (45). This mouse had also been injected with Hoechst 33342, 10,000 mol wt fluorescein dextran, and 500,000 mol wt rhodamine dextran, which labeled cell nuclei, endosomes of the proximal tubule, and the blood plasma, respectively. This image is a single frame from a 6-s series of images collected every 0.5 s, which is shown as Movie 5*d*. In this and other time series observations, many fluorescent leukocytes were detected flowing rapidly through the small vessels perfusing the renal cortex.

DISCUSSION

Use of two-photon microscopy for intravital studies of the kidney. When applied to living animals, optical microscopy can provide a powerful, noninvasive means of evaluating cell biology in the most physiologically relevant setting. Whereas early studies were primarily directed at studies of blood flow and leukocyte dynamics, the ability of two-photon microscopy to collect optical sections deep into biological tissues opened up the field of intravital microscopy to high-resolution studies of the brain, lens, skin, and tumors. In each case, two-photon microscopy provided physiological and morphological data at a spatial and temporal resolution orders of magnitude finer than that accessible through other intravital techniques such as magnetic resonance imaging or positron emission tomography. Studies of embryonic development (35) and neural development (24) indicate that two-photon microscopy may be performed on living animals with minimal perturbation of delicate biological processes.

Here we describe studies demonstrating numerous ways that intravital two-photon microscopy can be applied to various aspects of renal biology. Studies of animals injected with nuclear dyes may be used to assess acute effects of insults on cell necrosis and apoptosis.
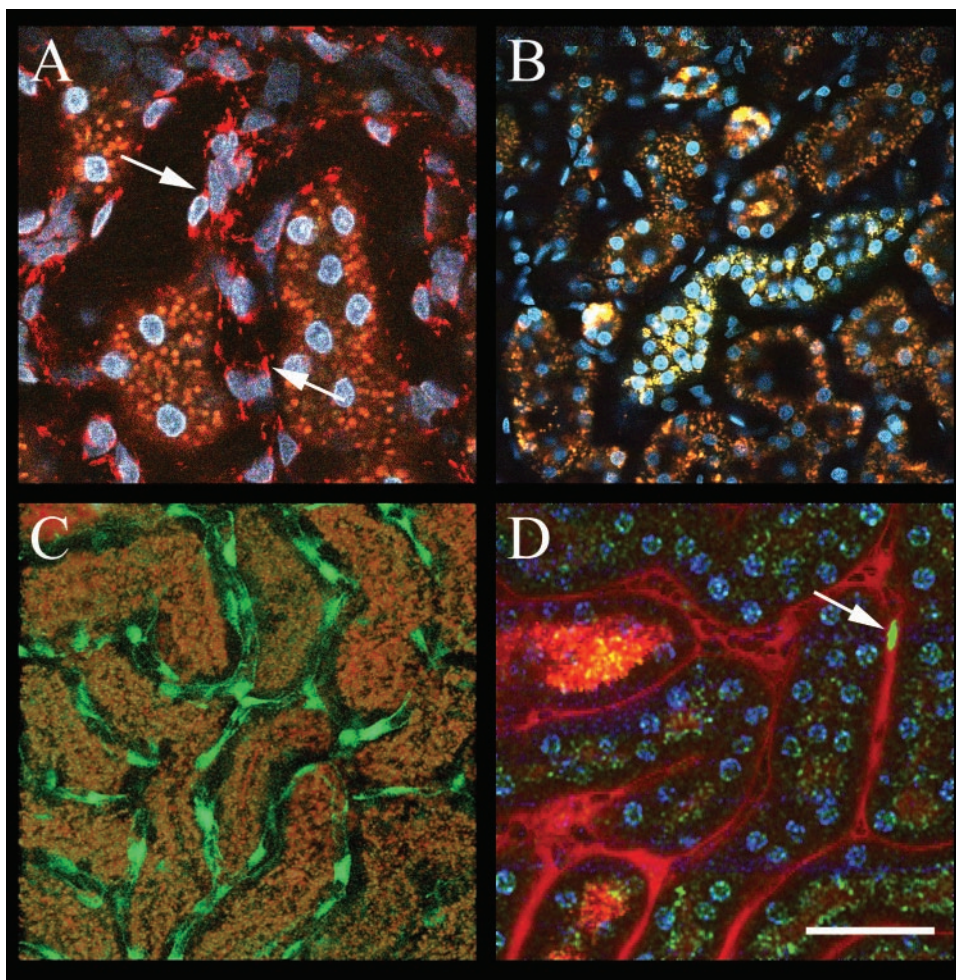
Fig. 5. Intravital fluorescence microscopy using potential-sensitive mitochondrial dyes and expression of GFP. *A*: image of the kidney of a living rat following intravenous injection of rhodamine R6 and Hoechst 33342 shows accumulation of rhodamine R6 in mitochondria of endothelial cells (arrows). Note that the red fluorescence of rhodamine R6 in endothelial cells can be clearly distinguished from the brown autofluorescent inclusions of the adjacent proximal tubule cells. *B*: image of the kidney of a rat following micropuncture delivery of 500,000 mol wt fluorescein dextran into the lumen of proximal tubule. In addition to the fluorescein dextran fluorescence in the endosomes of proximal tubule cells, the field also shows several tubular lumens with the orange fluorescence of the Sudan black-stained castor oil used to locate microinjected tubules. *C*: projection of a 3-dimensional volume collected from the kidney of a living transgenic mouse expressing GFP driven by an endothelial-specific promotor (Tie-2). The microvasculature, as delineated by the GFP-expressing endothelial cells, is shown surrounding renal cortical proximal tubules that, as in rats, contain brown autofluorescent inclusions. This volume is also presented as Movie 5*c*. *D*: image of the kidney of a mouse transplanted with bone marrow cells expressing enhanced GFP. This image is a single frame from a time series of images collected every 0.5 s showing the rapid movement of leukocytes through peritubular capillaries (Movie 5*d*). The arrow indicates one such leukocyte. This mouse had also been injected with Hoechst 33342, 500,000 mol wt rhodamine dextran, and 10,000 mol wt fluorescein dextran. Note that the 500,000 mol wt rhodamine dextran was not sufficiently dialyzed for this study; consequently, small molecular weight components apparently present in this probe were filtered through the glomeruli into tubules. Scale bar = 25 μm in *A*, 50 μm in *B*, and 40 μm in *C* and *D*.

Studies of animals injected with bulk fluid probes may be used to evaluate blood flow, glomerular filtration, and tubular transit and transport in individual segments. The kinetics of receptor-mediated endocytosis may be evaluated by injection of filtered ligands. Intravenously injected potential-sensitive dyes may be used to evaluate the energy state of individual cells. Finally, the acute behaviors of individual types of cells (e.g., inflammatory responses of endothelia and leukocytes) may be evaluated through the use of animals expressing fluorescent chimeras in specific cell types. In each case, intravital microscopy provides for unique physiological characterizations at subcellular spatial resolution, with subsecond temporal resolution while also providing crucial information about cell-cell variability in response.

Although the titanium-sapphire laser of our system can be tuned over a range from ~760 to 920 nm, imaging is conducted with the laser tuned to a particular narrow range of wavelengths. While this might appear to limit the ability to simultaneously image more than one fluorophore when using two-photon microscopy, two-photon excitation of commonly used

fluorophores occurs over a wide range of wavelengths, and thus multiple fluorophores may be efficiently excited by a single wavelength of light (47). The ability of our two-photon system to simultaneously collect three colors of fluorescence not only permitted the comparison of multiple probes and simultaneous characterization of multiple parameters but was also critical to evaluating specimens with varying amounts of endogenous autofluorescence. These punctate brown-fluorescing structures, which were only found in proximal tubule cells, displayed a characteristic fluorescent spectrum that reliably distinguished them from structures labeled with introduced fluorophores.

As with any other type of fluorescence microscopy, the simultaneous excitation of multiple fluorophores results in significant "bleed-through" of signals between detector channels. Although we could easily distinguish multiple probes in our implementation, in some cases this bleed-through might compromise the ability to compare the relative distributions of multiple probes. More sensitive discrimination of multiple probes can be accomplished by evaluating the emission spectrum of each pixel in an image, an approach used to distinguish two color variants of GFP (21) and to distinguish two sources of skin autofluorescence (25). Systems have recently become commercially available that combine instrumentation to collect spectroscopic image data with software designed to deconvolve the spectra into the individual fluorescence components.

Challenges of intravital two-photon microscopy. Multiphoton microscopy provides the means to collect images of cells and tissues in living animals at submicron resolution. However, intravital microscopy entails various difficulties not encountered in studies of cultured cells (24).

First, animal well-being is a primary concern for any study of living animals. Animals must be properly anesthetized and maintained, for both ethical and scientific reasons. This is particularly challenging for studies in which a tissue is to be analyzed over time. In many cases surgical techniques must be developed to provide access to particular areas without compromising the tissue perfusion, innervation, or function.

Second, high-resolution imaging requires that the sample volume be immobilized, which for studies of living animals entails not only anesthesia but also methods that minimize sample movement induced by respiration and the pulse during image capture. This problem is aggravated in current commercial two-photon systems that acquire images relatively slowly. Several new high-speed two-photon systems have been described (3, 13, 27), but these are not yet commercially available. These high-speed systems would facilitate kinetic analyses, perhaps even enabling three-dimensional studies. Although we have shown here that samples can be sufficiently immobilized to permit collections of image volumes comprising more than 80 optical sections, collection of such a volume generally takes a few minutes, which is unacceptably slow for characterizing rapid physiological events.

Third, studies of living animals are complicated by the difficulty of delivering probes to specific cells within organs. The problem of probe delivery may be avoided either by expressing fluorescent protein chimeras or by characterizing the fluorescence of endogenous molecules, some of which are environmentally sensitive and thus may be used to evaluate physiology quantitatively (1, 31).

Our studies of animals injected with bulk fluid probes demonstrate that intravenous injection is particularly useful for studies of fluid transport, where the redistribution of probes following intravenous injection provides an assay of glomerular filtration and tubular flow. The vascular route followed by fluorescent probes after intravenous injection, however, may not adequately label specific target cells. For example, we have been unable to deliver membrane-permeant probes such as rhodamine R6 and various acetoxymethyl esters (e.g., probes that could be used to measure intracellular pH and calcium concentrations) to renal tubule epithelial cells. Local delivery of these probes to tubule cells can be accomplished by tubular microinjection, which can also be used to deliver substances that are too large to pass the glomerular filtration barrier, such as large proteins, viruses, and liposomes. Thus micropuncture may be a valuable way of fluorescently labeling kidney tubules, pharmacologically manipulating single tubules, and delivering viral genetic vectors to tubular segments.

Tubular microinjection has several additional advantages over intravenous injection. Microinjection of a small amount of a drug avoids systemic effects and also limits the cost, which could be prohibitive of using drug doses appropriate for the whole animal. The concentration of microinjected substances in the tubule lumen may be precisely controlled. Finally, uninjected nephrons in the same kidney provide controls for the effects of injected reagents.

A fourth issue is that the scattering of light by biological tissues limits the depth into which tissues may be imaged. As discussed above, two-photon microscopy has extended the depth beyond that achievable by confocal microscopy so that high-resolution optical sections have been collected hundreds of micrometers into brain tissue (9, 14, 19, 37, 38). Nonetheless, light scatter ultimately limits imaging depth of two-photon systems as well. Because the resolution of two-photon images is relatively unaffected by scattering (5), additional depth can be reached by simply increasing the level of illumination (19). However, the solution of increased illumination must be approached with caution because nonlinear increases in tissue photodamage (16, 20) and disproportionate increases in photobleaching (29) are observed at higher levels of illumination. To some degree, the depth of imaging can be increased by modifying the optics of two-photon systems to improve the efficiency of light collection, which can be optimized without regard for optical aberrations, because fluorescence need not be imaged but simply collected in two-photon systems (28).

Future prospects for intravital two-photon microscopy. Intravital microscopy provides a unique window into cell biology in the most meaningful context: inside living animals. The studies described here demonstrate how two-photon microscopy can provide a level of resolution previously unattainable in intravital microscopy, enabling kinetic analyses and physiological studies in living animals with subcellular resolution. We have demonstrated the utility of two-photon microscopy for studies of the kidney, but we have used the same general approach to image the liver, pancreas, prostate, lung, and spleen. Thus two-photon microscopy will provide a powerful tool for studying cells and tissues of a variety of organs.

Two-photon microscopy is a relatively new technique, having been first described in 1990 (10, 11) with commercial systems not available until 1996. Because of this and the expense of commercial systems, relatively few biomedical laboratories have had access to two-photon systems. Nonetheless, two-photon microscopy is growing rapidly. Indeed, a literature search indicates that the number of published reports mentioning two-photon microscopy closely fits an exponential function of time since 1993, one that predicts that the next two years will see a doubling in the total number.

Another consequence of the recency of two-photon microscopy is that it is a relatively immature technology, particularly relative to biological imaging. The utility of two-photon microscopy will be improved as the unique optics and photophysics of two-photon microscopy are better understood and incorporated into the design of instruments and fluorescent probes. The utility of two-photon microscopy for intravital imaging will also evolve as biomedical researchers imagine new ways to exploit this powerful technique.

REFERENCES

1. **Bennett B, Jetton T, Ying G, Magnuson M, and Piston DW.** Quantitative subcellular imaging of glucose metabolism within intact pancreatic islets. *J Biol Chem* 271: 3647–3651, 1996.

2. **Brown BE, Campbell RB, Yoshikazu T, Lei X, Carmeliet P, and Rakesh KJ.** In vivo measurement of gene expression, angiogenesis and physiological function in tumors using multiphoton laser scanning microscopy. *Nat Med* 7: 864–868, 2001.

3. **Buehler C, Kim K, Dong C, Masters B, and So P.** Innovations in two-photon deep tissue microscopy. *IEEE Eng Med Biol Mag* 18: 23–30, 1999.

4. **Buhrle C, Hackenthal E, Helmchen U, Lackner K, Nobiling R, Steinhausen M, and Taugner R.** The hydronephrotic kidney of the mouse as a tool for intravital microscopy and in vitro electrophysiological studies of renin-containing cells. *Lab Invest* 54: 462–472, 1986.

5. **Centonze V and White J.** Multiphoton excitation provides optical sections from deeper within scattering specimens than confocal imaging. *Biophys J* 75: 2015–2024, 1998.

6. **Chen B, Lendvai B, Nimchinsky E, Burbach B, Fox K, and Svoboda K.** Imaging high-resolution structure of GFP-expressing neurons in neocortex in vivo. *Learn Mem* 7: 433–441, 2000.

7. **Clendenon JL, Phillips CL, Sandoval RM, Fang S, and Dunn KW.** Voxx: a PC-based, near real-time volume rendering system for biological microscopy. *Am J Physiol Cell Physiol* 282: C213–C218, 2002.

8. **Clemens M and Zhang J.** Regulation of sinusoidal perfusion: in vivo methodology and control by endothelins. *Semin Liver Dis* 19: 383–396, 1999.

9. **Denk W, Delaney K, Gelperin A, Kleinfeld D, Strowbridge B, Tank D, and Yuste R.** Anatomical and functional imaging of neurons using two-photon laser scanning confocal microscopy. *J Neurosci Methods* 54: 151–162, 1994.

10. **Denk W, Piston DW, and Webb WW.** Two-photon molecular excitation in laser-scanning microscopy. In: *Handbook of Biological Confocal Microscopy* (2nd ed.), edited by Pawley JB. New York: Plenum, 1995, p. 445–458.

11. **Denk W, Strickler J, and Webb WW.** Two-photon laser scanning fluorescence microscopy. *Science* 248: 73–76, 1990.

12. **DeVriese A, Endlich K, Elger M, Lamiere N, Atkins R, Lan H, Rupin A, Kriz W, and Steinhausen M.** The role of selectins in glomerular leukocyte recruitment in rat anti-glomerular basement membrane glomerulonephritis. *J Am Soc Nephrol* 10: 2510–2517, 1999.

13. **Fan G, Fujisake H, Miyawaki A, Tsay RK, Tsien R, and Ellisman M.** Video-rate scanning two-photon excitation fluorescence microscopy, and ratio imaging with cameleons. *Biophys J* 76: 2412–2420, 1999.

14. **Helmchen F, Svoboda K, Denk W, and Tank D.** In vivo dendritic calcium dynamics in deep-layer cortical pyramidal neurons. *Nat Neurosci* 2: 989–996, 1999.

15. **Heuser M, Seseke F, Zoller G, Gross A, Kugler A, Stojanovoc T, and Hemmerlein B.** Differences in cortical microcirculation in the kidneys of unilaterally congenital hydronephrotic rats. *Microvasc Res* 62: 172–178, 2001.

16. **Hopt A and Heher E.** Highly nonlinear photodamage in two-photon fluorescence microscopy. *Biophys J* 80: 2029–2036, 2001.

17. **Hudetz A.** Blood flow in the cerebral capillary network: a review emphasizing observations with intravital microscopy. *Microcirculation* 4: 233–252, 1997.

18. **Kelly KJ, Plotkin Z, and Dagher PC.** Guanosine supplementation reduces apoptosis and protects renal function in the setting of ischemic injury. *J Clin Invest* 108: 1291–1298, 2001.

19. **Kleinfeld D, Mitra P, Helmchen F, and Denk W.** Fluctuations and stimulus-induced changes in blood flow observed in individual capillaries in layers 2 through 4 of rat neocortex. *Proc Natl Acad Sci USA* 95: 15741–15746, 1998.

20. **Koester JH, Baur D, Ulh R, and Hell SW.** Ca^{2+} fluorescence imaging with pico- and femtosecond two-photon excitation: signal and photodamage. *Biophys J* 77: 2226–2236, 1999.

21. **Lansford R, Bearman G, and Fraser S.** Resolution of multiple green fluorescent protein color variants and dyes using two-photon microscopy and imaging spectroscopy. *J Biomed Opt* 6: 311–318, 2001.

22. **Lencer W, Weyer P, Verkman A, Ausiello D, and Brown D.** FITC-dextran as a probe for endosome function and localization in kidney. *Am J Physiol Cell Physiol* 258: C309–C317, 1990.

23. **Lendvai B, Stern E, Chen B, and Svoboda K.** Experience-dependent plasticity of dendritic spines in the developing rat barrel cortex in vivo. *Nature* 404: 876–881, 2000.

24. **Lichtman J and Fraser S.** The neuronal naturalist: watching neurons in their native habitat. *Nat Neurosci* 4: 1215–1220, 2001.

25. **Masters B, So P, and Gratton E.** Multiphoton excitation fluorescence microscopy and spectroscopy of in vivo human skin. *Biophys J* 72: 2405–2412, 1997.

26. **Motoike T, Loughna S, Perens E, Roman BL, Liao W, Chau TC, Richardson CD, Kawate T, Kuno J, Weinstein BM, Stainier DYR, and Sato TN.** Universal GFP reporter for the study of vascular development. *Genesis* 28: 75–81, 2000.

27. **Nguyen QT, Callamaras N, Hsieh C, and Parker I.** Construction of a two-photon microscope for video-rate Ca^{2+} imaging. *Cell Calcium* 30: 383–393, 2001.

28. **Oheim M, Beaurepaire E, Chaigneau E, Mertz J, and Charpak S.** Two-photon microscopy in brain tissue: parameters influencing imaging depth. *J Neurosci Methods* 111: 29–37, 2001.

29. **Patterson G and Piston D.** Photobleaching in two-photon microscopy. *Biophys J* 78: 2159–2162, 2000.

30. **Phillips C, Arend L, Kojetin D, Filson A, Clendenon J, Fang S, and Dunn KW.** 3-D imaging of embryonic mouse kidney by two-photon microscopy. *Am J Pathol* 158: 49–55, 2001.

31. **Piston DW, Masters B, and Webb WW.** 3-dimensional resolved NAD(P)H cellular metabolic redox imaging of the in situ cornea with two-photon excitation laser scanning microscopy. *J Microsc* 178: 20–27, 1995.

32. **Sandoval RM, Dunn KW, and Molitoris BA.** Aminoglycosides traffic rapidly and directly to the Golgi complex in LLC-PK1 cells. *Am J Physiol Renal Physiol* 279: F884–F890, 2000.

33. **Sandoval RM, Leiser JD, and Molitoris BA.** Aminoglycoside antibiotics traffic to the Golgi Complex in LLC-PK1 cells. *J Am Soc Nephrol* 9: 167–174, 1998.

34. **Schafer K, Gretz N, Bader M, Oberbaumer I, Eckardt KU, Kriz W, and Bachmann S.** Characterization of the Han:SPRD rat model for hereditary polycystic kidney disease. *Kidney Int* 46: 134–152, 1994.

35. **Squirrell J, Wokosin D, White J, and Bavister B.** Long-term two-photon fluorescence imaging of mammalian embryos without compromising viability. *Nat Biotechnol* 17: 763–767, 1999.

36. **Steinhausen M, Muller P, Parekh N.** Renal test dyes. IV. Intravital fluorescence microscopy and microphotometry of the tubularly secreted dye sulfonefluorescein. *Pflügers Arch* 364: 83–89, 1976.

37. **Svoboda K, Denk W, Kleinfled D, and Tank D.** In vivo dendritic calcium dynamics in neocortical pyramidal neurons. *Nature* 385: 161–165, 1997.

38. **Svoboda K, Tank D, and Denk W.** Direct measurement of coupling between dendritic spines and shafts. *Science* 272: 716–719, 1996.

39. **Tanner GA.** Nephron obstruction and tubuloglomerular feedback. *Kidney Int* 22: 213–218, 1982.

40. **Tanner GA, Gretz N, Shao Y, Evan A, and Steinhausen M.** Organic anion secretion in polycystic kidney disease. *J Am Soc Nephrol* 8: 1222–1231, 1997.

41. **Tanner GA and Knopp L.** Glomerular blood flow after single nephron obstruction in the rat kidney. *Renal Fluid Electrolyte Physiol* 250: F77–F85, 1986.

42. **Tanner GA and Steinhausen M.** Tubular obstruction in ischemia-induced acute renal failure in the rat. *Kidney Int* 6: S64–S73, 1976.

43. **Uhlmann S, Uhlmann D, and Spiegel H.** Evaluation of hepatic microcirculation by in vivo microscopy. *J Invest Surg* 12: 179–193, 1999.

44. **Vajkoczy P, Ullrich A, and Menger M.** Intravital fluorescence microscopy to study tumor angiogenesis and microcirculation. *Neoplasma* 2: 53–61, 2000.

45. **Williams DA, Tao W, Yang F, Kim C, Gu Y, Mansfield P, Levine JE, Petryniak B, Derrow CW, Harris C, Jia B, Zheng Y, Ambruso DR, Lowe JB, Atkinson SJ, Dinauer MC, and Boxer L.** Dominant negative mutation of the hematopoietic-specific Rho GTPase, Rac2, is associated with a human phagocyte immunodeficiency. *Blood* 96: 1646–1654, 2000.

46. **Winet H.** The role of microvasculature in normal and perturbed bone healing as revealed by intravital microscopy. *Bone* 19: 39S–57S, 1996.

47. **Xu C, Williams R, Zipfel W, and Webb WW.** Multiphoton excitation cross-sections of molecular fluorophores. *Proc Natl Acad Sci USA* 4: 198–207, 1996.